P13A.17 DOPPLER RADAR OBSERVATIONS OF THE INTERACTIONS OF GRAVITY WAVES WITH MESOCYCLONES

Timothy A. Coleman* and Kevin R. Knupp
The University of Alabama, Huntsville, Alabama

1. INTRODUCTION

Several cases in which a mesocyclone intensifies upon interaction with one or more apparent mesoscale gravity waves have been observed in the southeastern United States. These interactions, as well as the kinematics of gravity waves in general, are being studied using Doppler radar data.

Interactions between gravity waves and convection have been investigated by many authors (e.g., Uccellini 1975; Stobie et al. 1983; Koch et al. 1988; Cram et al. 1992). However, the interactions between gravity waves and mesocyclones have received limited attention, and most of it has been observational (e.g., Miller and Sanders 1980; Kilduff 1999; Barker 2006). Coleman and Knupp (2006) propose an initial theory for the interactions.

In this paper, a brief review of ducted gravity waves will be presented, along with Doppler radar observations of waves, including vertical cross-sections and VAD wind profiles. The theory and modeling of wave interactions with a mesocyclone will be reviewed. Finally, radar observations of gravity waves interacting with a mesocyclone will be presented and compared to theory.

2. DUCTED GRAVITY WAVES

2.1 *Theory*

Gravity waves may be generated by many processes, including convection, geostrophic adjustment, topography, and shear instability (Koch and O'Handley 1997). Internal gravity waves may be described by the wind perturbations (u') associated with them, ie.,

$$u' = A\cos(kx + mz - \omega t) \qquad (1)$$

where A is the wave amplitude, k=2π/λ_x is the horizontal wavenumber, m=2π/λ_z is the vertical wavenumber, and ω is the frequency. The above expression represents an upward-propagating wave; a downward propagating wave would be represented by a similar expression with a minus sign associated with the mz. Waves may be reflected by the ground, or by atmospheric layers in which there is a large vertical gradient in m, related to static stability and wind shear (e.g., Nappo 2002).

Without a "duct" in place, wave energy would leak rapidly upward, preventing the maintenance of a coherent wave. However, Lindzen and Tung (1976) showed that a wave may be "ducted" by a stable layer near the surface, provided the stable layer is deep enough to accommodate ¼ of the vertical wavelength, contains no critical level, and is topped by a conditionally unstable layer. They also showed that the *intrinsic* phase speed for a ducted wave is given by c-U = $2ND\pi^{-1}$, where c is the ground-relative wave phase speed, U is the mean wave normal wind component in the duct, N is the Brunt-Vaisala frequency, and D is the depth of the stable duct.

Wave reflection occurs at the top of the duct and at the ground. When the duct depth is equal to ¼ of the vertical wavelength, the upward and downward moving waves constructively interfere, as shown in Figure 1. A ducted wave is then made up of two waves which constructively interfere, one of which is propagating upward and one propagating downward (e.g., Nappo 2002, Lindzen 2007, personal communication).

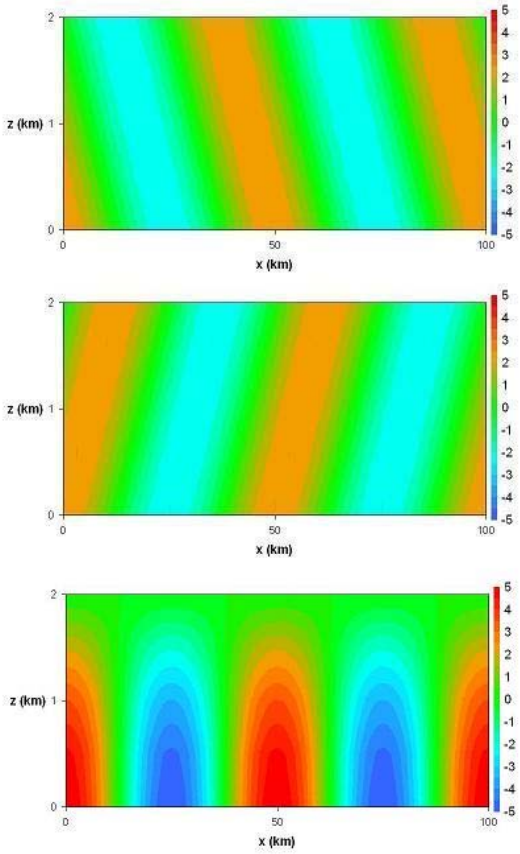

Figure 1. u' (m s^{-1}) in components of ducted wave traveling to the right. Upward propagating wave (top), downward propagating reflected wave (middle), and superposed upward and downward propagating waves (bottom). The horizontal wavelength is 50 km, and the vertical wavelength is 8 km.

*Corresponding Author Address: Timothy A. Coleman, Atmospheric Science Department, The University of Alabama in Huntsville, 320 Sparkman Drive, Huntsville, AL 35805; Email: coleman@nsstc.uah.edu.

Significant divergence and vertical wind shear are associated with the wind perturbations in a ducted gravity wave. *The divergence is largest near the surface*, with convergence ahead of the wave ridge and divergence ahead of the wave trough. *The vertical shear is largest near the top of the duct*, with positive shear centered at the wave trough and negative shear centered at the wave ridge. The perturbation divergence and vertical wind shear are illustrated in Figure 2, and are fairly consistent with those illustrated by the schematic of an idealized linear plane gravity wave from Bosart and Sanders 1986 (see Figure 3).

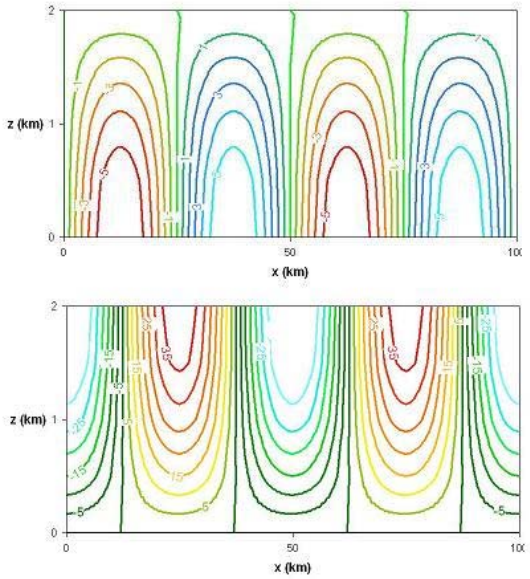

Figure 2. Horizontal divergence (top, in units of 10^{-4} s^{-1}, blue shades illustrate divergence and red shades illustrate convergence) and vertical shear (bottom, in units of 10^{-4} s^{-1}, blue shades illustrate negative shear and red shades illustrate positive shear) associated with the wind perturbations in the gravity waves shown In Figure 1.

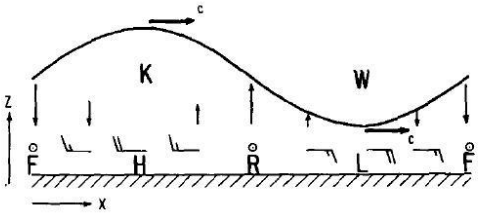

Figure 3. Schematic of a linear plane gravity wave (Bosart and Sanders 1986, after Eom 1975).

2.2 *Radar Observations*

The kinematics of a ducted gravity wave which moved through northeast Alabama on 10 May 2006 were analyzed using Doppler radar data. This analysis was then compared to the idealized wave discussed above. The wave is evident in surface pressure data as a wave of depression. The wave was moving from 250 degrees at 22 m s^{-1}, in excellent agreement with the speed predicted using proximity sounding data and the ducted wave speed equation from Lindzen and Tung (1976) of 20.8 m s^{-1}. The top of the duct is about 1500 m MSL.

First of all, vertical cross-sections of horizontal wind perturbation were generated as the wave approached the KHTX WSR-88D radar. These cross-sections were produced using Level-II NEXRAD data along an azimuth normal to wave motion. The data were converted to a Cartesian grid. Given the radial velocity, elevation angle, and reflectivity at each grid point, the horizontal wind was computed at each point. This allowed computation of divergence and vertical wind shear.

The results (shown in Figure 4) are, at least qualitatively, in excellent agreement with theory. Note first of all the maximum wind perturbation co-located

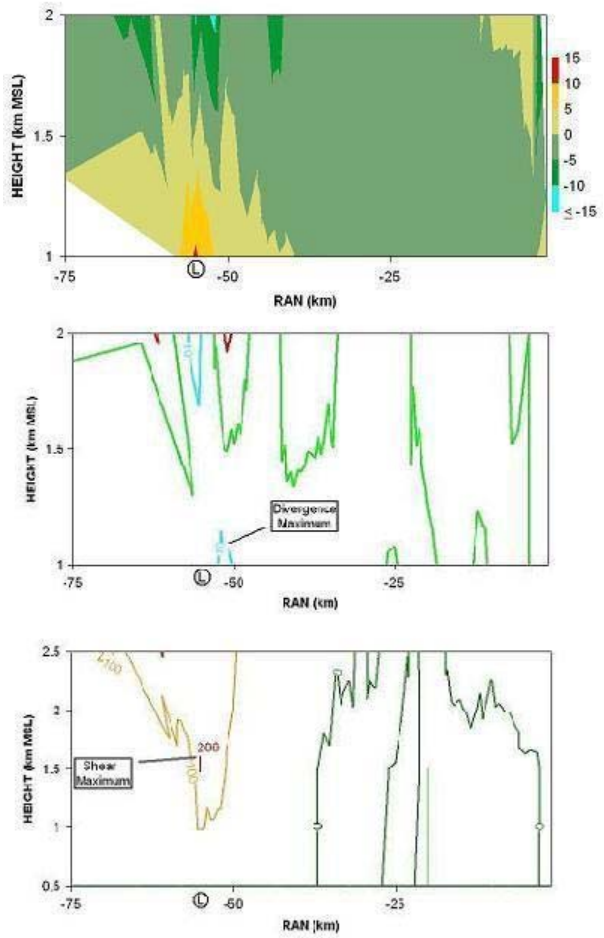

Figure 4. Radar-derived vertical cross-section of *u'* (top, m s^{-1}), divergence (middle, 10^{-4} s^{-1}), and vertical wind shear (bottom, 10^{-4} s^{-1}). KHTX radar, azimuth 250 degrees, 1845 UTC, 10 May 2006.

with the wave trough, indicated by the "L" with a circle around it. Note also that the maximum divergence is near the surface and ahead of the wave trough. Maximum vertical wind shear is at the wave trough, near the height of the top of the duct (1500 m MSL, determined using sounding data).

The perturbation vertical shear and divergence also shows up very well in WSR-88D VAD wind profiles based on data from KHTX (Figure 5). The wave trough passed the radar site around 1945 UTC. Note that the low-level flow is backing rapidly with time, in response to the approaching perturbation wind maximum (perturbation winds in the trough are from the ENE, opposite the direction of wave motion). Time-to-space conversion indicates low-level divergence.

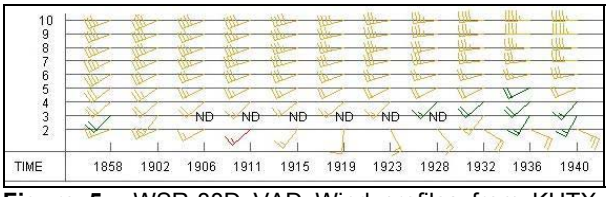

Figure 5. WSR-88D VAD Wind profiles from KHTX, 1858-1940 UTC, 10 May 2006.

As the trough approaches, vertical wind shear is also increasing rapidly. Ground-relative helicity increases from near 0 at 1845 to greater than 200 m^2s^{-2} by 1945.

3. DYNAMICS OF THE INTERACTIONS OF WAVES WITH MESOCYCLONES

3.1 *Theory*

The following is a review of the theory and numerical modeling of the interactions of gravity waves with mesocyclones introduced by Coleman and Knupp (2006).

The time rate of increase in vertical vorticity following the motion, neglecting solenoidal effects and friction, is related to the stretching of pre-existing vorticity by horizontal convergence, and the tilting of horizontal vorticity into the vertical.

In a ducted plane gravity wave, convergence is maximized 90 degrees ahead of the wave ridge, and divergence is maximized 90 degrees ahead of the wave trough (see Figure 2). Convergence can not create vorticity where there is none, but it can enhance pre-existing vorticity. So, one would expect the vorticity to increase ahead of the wave ridge, and decrease ahead of the wave trough. Interaction with the convergent part of a gravity wave may easily double the vorticity within a mesocyclone.

It has been shown above that significant perturbation wind shear may accompany a ducted gravity wave, which significantly alters the environmental wind profile and helicity. The potential effect on a mesocyclone may be estimated using the tilting term in the vorticity equation, in a wave-normal coordinate system, which may be written as

$$\frac{D\zeta}{Dt} = \left(\frac{\partial u'}{\partial z}\right)\left(\frac{\partial w}{\partial y}\right)\sin\alpha \qquad (2)$$

where w is vertical motion, x is in the direction of wave motion and y is orthogonal and to its left, and α is the angle between the wave vector and the mean storm-inflow in the duct. α must be considered, since only the *streamwise* portion of the wave-induced horizontal vorticity will contribute to the net vorticity of the mesocyclone.

3.2 *A combined numerical model*

A numerical model is under development to simulate the interaction of a gravity wave with a pre-existing mesocyclone. The simple model discussed by Coleman and Knupp (2006) considers only the stretching and tilting processes. This model is currently being modified somewhat, but it works fairly well and will be applied here for discussion purposes. Suppose a storm containing a mesocyclone of initial vorticity 1 $x10^{-2}$ s^{-1} interacts with a gravity wave. For the wave, c=25 m s^{-1}, λ_x=50 km, its duct depth is 2000 m, and u'_{MAX}=15 m s^{-1}. The model-simulated vorticity change with time is depicted in Figure 6. t=0 is taken as the time 90 deg ahead of the wave trough, and the model allows one full wavelength to pass the through the mesocyclone.

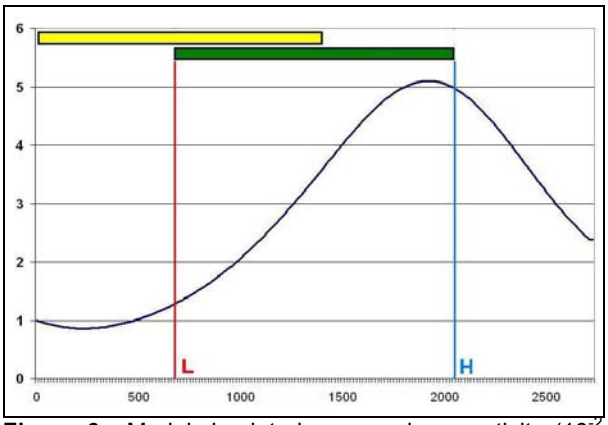

Figure 6. Model-simulated mesocyclone vorticity (10^{-2} s^{-1}) vs. time (s). **L** and **H** represent the wave trough and ridge passage, respectively. The yellow bar indicates the region of constructive vorticity tilting, and the green bar indicates positive vorticity stretching. The horizontal scale of the figure indicates a full horizontal wavelength.

In this model, vorticity increases to a maximum value near 5 x 10^{-2} s^{-1} just ahead of the wave ridge, and even after one full wave period, the vorticity is higher than the initial vorticity. This is a fascinating result.

4. RADAR OBSERVATIONS OF INTERACTIONS

4.1 *22 January 1999, Northwest Alabama*

On 22 January 1999, a low-CAPE, high-shear environment existed over Alabama. The 1800 UTC sounding from Birmingham (BMX) indicates a shallow mixed layer topped by a rather deep stable layer, up to a height of about 1900 m MSL, with a layer of lower static stability above 1900 m MSL. Using the ducting theory of Lindzen and Tung (1976), this environment would support ducted gravity waves with ground-relative phase speeds around 37 m s^{-1}.

Severe convection moves into extreme western Alabama around 2000 UTC. Around the same time, *a pair of mesoscale gravity waves appear on radar as two thin bands of enhanced reflectivity.* These bands are classified as gravity waves, since the environment (synoptic and local) is favorable for their genesis and propagation, and since these bands are moving northward at 32 m s^{-1}, which is fairly close to the predicted 37 m s^{-1}.

Gravity waves are often detectable on radar, if the rising motion ahead of the wave ridge is sufficient to lift parcels to their lifted condensation level (LCL) and produce radar-detectable clouds and precipitation. Several studies (e.g., Uccellini 1975; Einaudi and Lalas 1975) have shown that gravity waves may produce condensation, and even initiate severe convection. The enhanced reflectivity associated with a gravity wave should show up near or just ahead of the wave ridge. This is supported by the observations of Miller and Sanders (1980), Sanders and Bosart (1985), and Koch et al. (1988). Studies have also shown that incipient gravity waves may remain coherent even in the presence of convection (e.g., Balachandran 1980; Koch et al. 1988).

The key in identifying a band of reflectivity on radar as a gravity wave is in its speed of motion. A density current may be ruled out using the speed equation developed by Seitter (1986). Surface observations of a pressure-wind correlation associated with the reflectivity band, consistent with the gravity wave impedance relation (e.g., Gossard and Hooke 1975), are also helpful.

An intense convective storm with a rather weak mesocyclone is shown in Figure 7. The two apparent gravity wave ridges are also visible. At the time of this image (2042 UTC), the initial wave ridge has just passed the mesocyclone, and the second wave, which appears more vigorous based on its radar reflectivity, is approaching the storm from the south. The second wave ridge intersects the mesocyclone around 2102 UTC, and the vorticity increases rapidly ahead of the wave ridge, reaching almost 2 x 10^{-2} s^{-1} by 2102 UTC, with gate-to-gate maximum inbound and outbound storm-relative velocities (see Figure 8). Shortly after 2102 UTC, a small tornado touched down in northern Fayette County, Alabama (the county containing the mesocyclone) (Kilduff 1999).

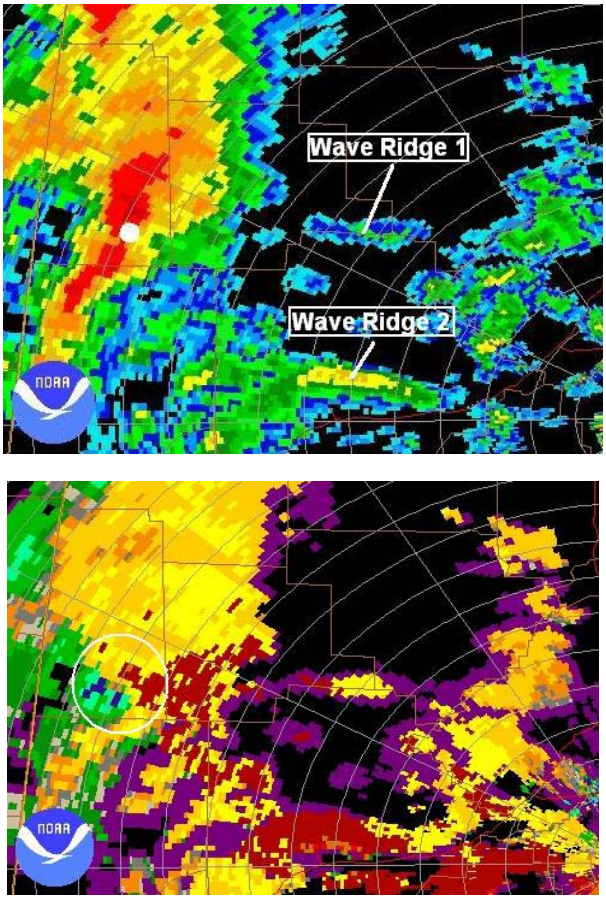

Figure 7. 2042 UTC 22 January 1999 0.5 deg reflectivity (top) and storm-relative velocity (bottom) from WSR-88D radar at Birmingham, AL (BMX).

Figure 8. 2102 UTC 0.5 deg storm-relative velocity (BMX) showing gate-to-gate maximized (magnitude > 50 kt, > 25 m s^{-1}) inbound and outbound velocities.

In this case, Doppler radar velocity data and mesocyclone diameter were used to estimate mesocyclone vorticity, and these results are plotted in Figure 9. Doppler radar data were also used to estimate the wind perturbations, speed, and wavelength of the gravity waves. The numerical model (Coleman and Knupp 2006) was then initialized using wave and

storm parameters, and results compared very well with what actually occurred (see Figure 10).

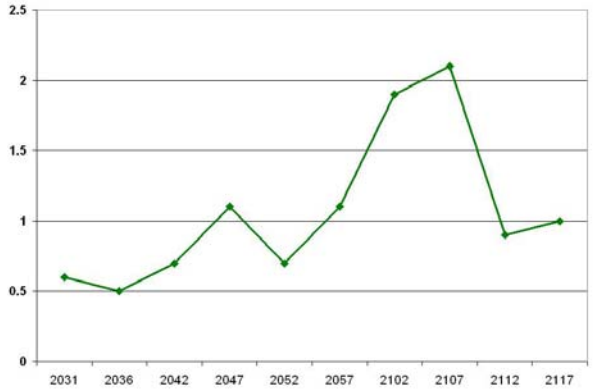

Figure 9. Mesocyclone vorticity estimated using Doppler velocity data.

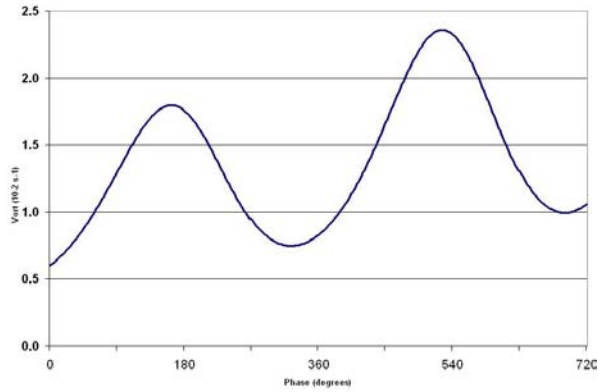

Figure 10. Model simulated vorticity.

4.2 *8 April 1998, Birmingham, Alabama*

On 8 April 1998, beginning around 7:52 pm CDT, an F5 tornado moved through parts of eastern Tuscaloosa and western Jefferson counties (in Alabama), including some of the western suburbs of Birmingham. With this tornado, there were 32 fatalities and 258 injuries (Pence and Peters 2000). Prior to the touchdown of this tornado, two or more parallel bands of enhanced reflectivity, possibly associated with an undular bore or gravity waves, were indicated on radar advancing toward the parent supercell (see Figure 11). Upon interaction with one of these reflectivity bands (around 0058 UTC), a tornado that was already on the ground producing a narrow path of F0 damage, quickly intensified and produced F3 damage, and the damage path became 1 km wide (Pence and Peters 2000).

Vertical cross-sections roughly normal to the reflectivity bands (Figure 12) show evidence of the wave ridges/bore, including enhanced reflectivity, and horizontally alternating patterns of convergence and divergence. This convergence may have played a role in the tornado's intensification.

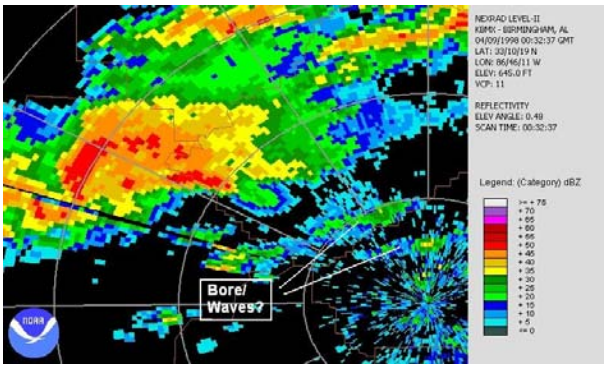

Figure 11. BMX WSR-88D reflectivity at 0033 UTC.

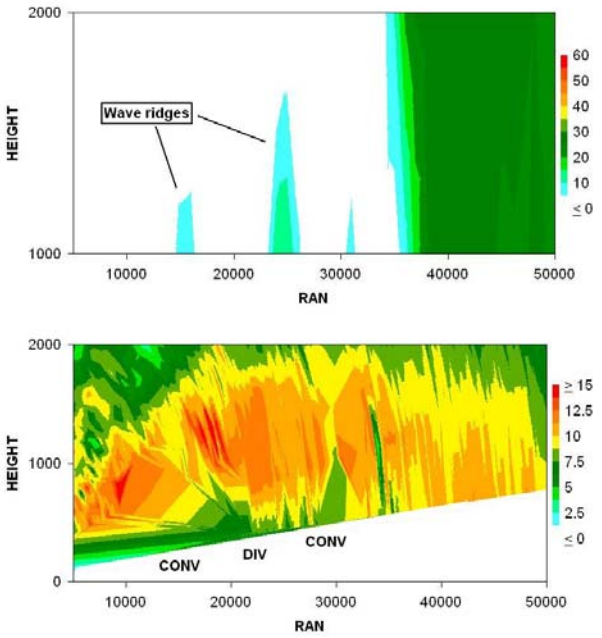

Figure 12. Vertical cross-sections of reflectivity (top) and un-gridded velocity (bottom) at 0033 UTC from BMX, at azimuth 330 degrees.

5. CONCLUSIONS

Gravity waves may significantly impact mesocyclones/tornadoes with which they interact. The wind perturbations within the wave alter the environmental wind shear, and through tilting allow vorticity to be produced in the mesocyclone, while the convergence ahead of the wave ridge helps to concentrate vorticity through stretching.

Doppler radar data, through vertical cross-sections of horizontal winds and VAD wind profiles, provide an important resource for the analysis of convergence and vertical wind shear associated with gravity waves. Velocity azimuth display (VAD) analysis at small radii may also contribute to the analysis of the kinematics of gravity waves, and is planned.

Doppler radar data also allow for analysis of the interactions of gravity waves with mesocyclones, including mesocyclone vorticity estimates, and wave characteristics. Analysis of the 22 January 1999 case shows excellent agreement with numerical simulations.

Perhaps most importantly, Doppler radar data allow for the real-time detection of potential interactions of a pre-existing mesocyclone with a gravity wave. Lifting ahead of wave ridges often produces a band of reflectivity on radar, and the speed of motion of the band may be estimated and compared to theoretical density current and gravity wave speeds, allowing for the identification of waves.

REFERENCES

Balachandran, N. K., 1980: Gravity waves from thunderstorms. *Mon. Wea. Rev.*, **108**, 804-816.

Barker, L. J., 2006: A potentially valuable WSR-88D severe storm pre-cursor signature in highly dynamic, low CAPE, high shear environments.

Bosart, L. F., and F. Sanders, 1986: Mesoscale structure in the Megalopolitan snowstorm of 11-12 February 1983. Part III: A Large amplitude gravity wave. *J. Atmos. Sci.*, **43**, 924-939.

Coleman, T. A., and K. R. Knupp, 2006: The interactions of gravity waves with tornadoes and mesocyclones: Theories and observations. *23rd Conf. on Severe Local Storms*, American Meteorological Society.

Cram, J. M., R. A. Pielke, and W. R. Cotton, 1992: Numerical simulation and analysis of a prefrontal squall line. Part II: Propagation of the squall line as an internal gravity wave. *J. Atmos. Sci.*, **49**, 209-225.

Einaudi, F., and D. P. Lalas, 1975: Wave-induced instabilities in an atmosphere near saturation. *J. Atmos. Sci.*, **32**, 536-547.

Eom, J.-K., 1975: Analysis of the internal gravity wave occurrence of 19 April 1970 in the Midwest. *Mon. Wea. Rev.*, **103**, 217-226.

Gossard, E. E., and W. H. Hooke, 1975: Gravity waves in the atmosphere. 475 pp.

Kilduff, R. E., 1999: The interaction of a gravity wave with a thunderstorm. Electronic poster, NOAA/National Weather Service.

Koch, S. E., and C. O'handley 1997: Operational forecasting and detection of mesoscale gravity waves. *Wea. Forecasting*, **12**, 253-281.

Koch, S. E., R. E. Golus, and P. B. Dorian, 1988: A mesoscale gravity wave event observed during CCOPE. Part II: Interactions between mesoscale convective systems and the antecedent waves. *Mon. Wea. Rev.*, **116**, 2545-2569.

Lindzen, R. S., 2007: Personal communication.

Lindzen, R. S., and K. –K. Tung, 1976: Banded convective activity and ducted gravity waves. *Mon. Wea. Rev.*, **104**, 1602-1617.

Miller, D. A., and F. Sanders, 1980: Mesoscale conditions for the severe convection of 3 April 1974 in the East-Central United States. *J. Atmos. Sci.,* **37,** 1041-1055.

Nappo, C. J., 2002: An introduction to atmospheric gravity waves. 276 pp.

National Weather Service, 2000: Tuscaloosa Tornado, on-line storm report.

Pence, K. J., and B. E. Peters, 2000: The tornadic supercell of 8 April 1998 across Alabama and Georgia. *20th Conf. on Severe Local Storms,* American Meteorological Society.

Sanders, F., and L. F. Bosart, 1985: Mesoscale structure in the Megalopolitan snowstorm, 11-12 February 1983. Part II: Doppler Radar Study of a New England snowband. *J. Atmos. Sci.*, **42,** 1398-1407.

Seitter, K. L., 1986: A numerical study of atmospheric density current motion including the effects of condensation. *J. Atmos. Sci.*, **43**, 3068-3076.

Stobie, J. G., F. Einaudi, and L. W. Uccellini, 1983: A case study of gravity waves-convective storms interaction: 9 May 1979. *J. Atmos. Sci.*, **40**, 2804-2830.

Uccellini, L. W., 1975: A case study of apparent gravity wave initiation of severe convective storms. *Mon. Wea. Rev.*, **103**, 497-513.